RSC Advances

ROYAL SOCIETY OF CHEMISTRY

www.rsc.org/advances

Cite this: DOI: 10.1039/c0xx00000x

www.rsc.org/xxxxxx

ARTICLE TYPE

Easy Amino-group Modification of Graphene Using Intermolecular Force for DNA Biosensing

Zhihong Zhang[1,2]*, Shunli Liu[1], Yuanchang Zhang[1], Mengmeng Kang[1], Linghao He[1], Xiaozhong Feng[1], Donglai Peng[1] and Peiyuan Wang[1]

Received (in XXX, XXX) Xth XXXXXXXXX 20XX, Accepted Xth XXXXXXXXX 20XX
DOI: 10.1039/b000000x

We demonstrated an easy and efficient approach to producing amino-group-functionalized graphene (G-NH_2) for highly sensitive DNA biosensing through intermolecular interaction. The nucleotide molecules prefer to anchor onto as-prepared G-NH_2 surface rather than be immobilized on pristine graphene. The electrostatic interaction between the positive charges of ionized amino on G-NH_2 and the negative charges of phosphate groups on nucleotide chains enabled label-free probe DNA to be immobilized on the G-NH_2 surface. The electrochemical performance and quality variations during the preparation of G-NH_2 and nucleotide immobilization processes were determined by electrochemical measurements and quartz crystal microbalance in situ, respectively. Results showed that complementary target DNA could be hybridized with probe DNA within the concentration range of 0.1 nM to 200 nM, and the detection limit was 0.8 nM. Therefore, this kind of G-NH_2 could be an alternative to DNA biosensing.

1. Introduction

As a new nanomaterial, graphene has excellent electric properties and a large specific surface area [1]. Theoretical research, preparation methods, and applications of graphene have been recently reported. The applications of graphene as biomaterials focus on the glucose oxidase or protein adsorption [2], DNA or aptamer immobilization [3], and cell adhesion [4]. The functionalization and dispersion of graphene can be improved by covalent [5] and non-covalent methods [6] because of the hydrophobicity and assemblage of graphene. Graphene functionalized with amino [7, 8], carboxyl [9], and doping functionalization [10], has good biocompatibility [11] and biological detection characteristics [12-14]. Graphene sheets functionalized covalently with the amino groups of poly-L-lysine, which provided a very biocompatible environment for attaching bioactive molecules[7]. Amino-functionalized graphene is prepared through the chemical modification of carboxyl groups introduced on the graphene surface followed by the deposition onto the gold nanoparticles and application on the adsorption of a catalyst [8].

The self-assembly approach is an important and effective strategy for nanofabrication. It has been extensively used to produce more efficient and functional materials [15]. Self-assembled hybrid nanostructures with an appropriate design can deliver synergistic effects resulting in highly directed materials [16]. Compared with chemical functionalization, self-assembly modification is simple, convenient, and with fewer defects.

Graphene can be a promising building block in the hybridization with various nanoparticles (NPs). However, only a small number of examples of graphene NP hybrids through self-assembly approaches have been reported. Fang et al. demonstrated the use of cationic polyelectrolyte poly (diallyldimethyl ammonium chloride) functionalized graphene nanosheets as building blocks in the self-assembly of graphene nanosheets and Au nanoparticle heterostructure resulting to an enhanced electrochemical catalytic ability [17]. Also, the positively and negatively charged graphene nanoplatelets assembled together forming a multilayer structure due to coulomb attraction between opposite charges [18].

The chemical method is mainly used to modify graphene by amino groups. Actually, it has some disadvantages, including the complicated reaction procedure, need for heating, and possibility of destruction of graphene surface [19, 20]. However, the self-assembling of the alkane molecules with short alkyl chains on graphene [21], such as tridecane ($C_{13}H_{28}$), tetradecane ($C_{14}H_{30}$), and pentadecane ($C_{15}H_{32}$), could result in the surface funtionality without destroying the properties of the bulk graphene. In consequence, layer-by-layer self-assembling technique [22] is used to fabricate the amino modified graphene that could be applied as the matrix of biosensors. The schematic of DNA immobilization and hybridization onto the surface of amino modified graphene (G-NH_2) by the self-assembling method is summarized in Scheme 1. The method involved two steps, i.e., the formation of G-NH_2 through the self-assembling approach and DNA anchoring.

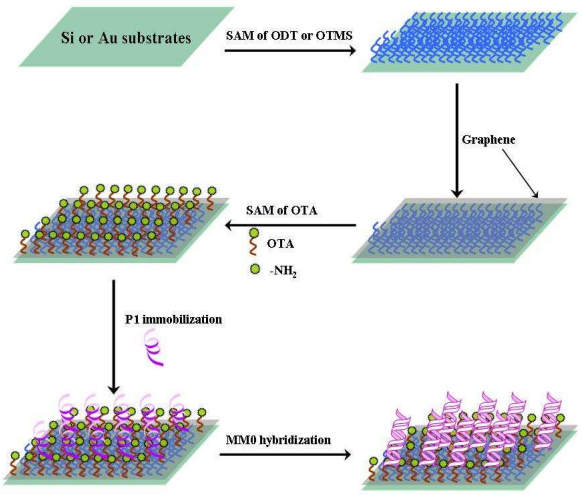

Scheme 1. Schematic diagram of DNA immobilization/ hybridization onto the surface of G-NH_2 via the intermolecular force.

First, octadecyltrimethoxysilane (OTMS) self-assembles onto silicon wafers through the silicon-oxygen bonds between OTMS and silicon [23]. In the case of Au substrates, 1-octadecanethiol (ODT) was used for self-assembly to form the Au-S bonds. Graphene bonds with the alkyl chain of OTMS through intermolecular force [24] and then alkyl chains of 1-octadecylamine (OTA) bonds with the graphene through the same bonding interaction. Finally, label-free DNA adheres to the surface of G-NH_2.

2. Materials and methods

2.1. reagents

Octadecyltrimethoxysilane, 1-octadecanethiol, 1-octadecylamine, were purchased from Aladdin (Shanghai, China). Graphene was purchased from JCNANO Co. Ltd. (Nanjing, China). DNA was obtained from Beijing SBS Genetech Co. Ltd. (Beijing, China). The probe oligonucleotide sequences are

Probe-DNA (P1, 30 mer): 5'-TTT TTT TTT TTT TTT TGT ACA TCA CAA CTA-3'

Total mismatch target DNA (TMM, 15mer): 5'-TGT GCC TAA GCC ATA-3'

Complementary target DNA (MM0, 15mer): 5'-TAG TTG TGA TGT ACA-3'

2.2. Preparation of the self-assembled films of amino-group modified graphene

Graphene and OTA were successively self-assembled with OTMS or ODT onto the silicon or Au wafers (See Scheme 1). The same self-assembling procedures were implemented, and ethanol was used as the solvent in the preparation of the self-assembling solution. The treated wafers (2 cm × 2 cm) were immersed into the self-assembling ethanol solution (10 mL : 0.1 mg/mL) for 2 h to 4 h, rinsed with Milli-Q H_2O, and dried with the high-pure nitrogen. The self-assembled films of G-NH_2 was fabricated and applied as the matrix for DNA immobilization and hybridization.

2.3. DNA Immobilization/hybridization on the surface of G-NH_2

In this study, the DNA solutions were created using phosphate buffer solution (PBS) at a pH of 7.4. DNA immobilization was performed in 1 μM P1 solution for 24 h. Before analysis, each sample was rinsed with PBS and Milli-Q H_2O and then dried under flowing nitrogen. Finally, the G-NH_2 immobilized with P1 was immersed in 1 μM target DNA solution for another 24 h and then rinsed with PBS and Milli-Q H_2O.

2.4. Characterization

Analysis of the surface electronic structure by X-ray photoelectron spectroscopy (XPS) was performed using VG ESCALAB HP photoelectron spectrometer equipped with the analyzer and the preparation chambers. X-ray source with power less than or equal to 100 W was used to record the spectra Al Kα ($h\upsilon$ = 1486.6 eV). Atomic force microscopy (AFM) was utilized to characterize the surface morphology of assembled nanofilms. Measurements were conducted in tapping mode by a Nanoman AFM (Veeco Metrology Group, USA) at ambient temperatures.

2.5. Electrochemical measurements

CHI600D series of the electrochemical workstation (Shanghai Chenhua, China) was used to test the self-assembly and DNA immobilization and hybridization processes. A conventional three-electrode cell was used, including an Ag/AgCl (saturated KCl) electrode as the reference electrode, platinum slides as the counter electrode, and Au film substrate as the working electrode. The electrochemical impedance spectroscopy (EIS) was obtained at a potential of –0.2 V_{MSE} at a frequency range of 10^6 Hz to 10^{-2} Hz with an AC amplitude of 5 mV. The spectra were then analyzed using the Zview2 software, which uses a non-linear least-squares fit to determine the parameters of the elements in the equivalent circuit.

2.6. Quartz crystal microbalance measurements

CHI440B series of electrochemical quartz crystal microbalance (QCM) (Shanghai Chenhua, China) was used to test the quality changes. QCM is a detectable change in nanogram quality, ultra-sensitive instruments. The basic principle of measure is the inverse voltage effect and Sauerbrey equation [29, 30]:

$$\Delta F = -[2f_0^2/(\mu_q \bullet \rho_q)^{1/2} A]\,\Delta m \qquad (1)$$

where ΔF is the frequency change, f_0 is the natural frequency of quartz crystal, μ_q is the density of quartz (2.648 g·cm^{-3}), ρ_q is the quartz shear modulus (2.947 × 1011 g·cm^{-1}·s^{-2}), A is the effective piezoelectric area, and Δm is the mass change on the substrate. f_0 and A are QCM device-specific parameters, the research group of f_0 using QCM is about 8.0 × 10^6 Hz, and A is 0.196 cm^2, which can be calculated in this research group QCM curve of -1 Hz = 1.34 ng.

3. results and discussion

3.1. Chemical components of G-NH_2 before and after DNA immobilization

XPS was used to determine the chemical components of self-assembling modified graphene before and after DNA immobilization (Fig. 1). The fits of C 1s contain four component peaks corresponding to the different chemical environments present in the sample. The peak at approximately 284.6 eV was assigned to C-C/C-H. The peak at approximately 285.6 eV is due to C-N, whereas the peak at approximately 286.1 eV has possible contributions from C-O (alcohol or ether). C-N groups should be from OTA bonded with graphene. Moreover, C-O groups could be observed in the OTMS and graphene. For the self-assembling modified graphene, the highest binding energy at 287.6 eV should be due to C=O (carbonyl) in graphene.

However, the peak at 287.6 eV after DNA immobilization has two possible contributions, namely, from C=O in graphene or N-C=O groups in the strands of DNA. In comparison with the content of the carbon-related groups in the amino modified graphene, the density of C-N groups substantially decreased from 32.6 % to 15.2 %, whereas that of the C-O and C=O or N-C=O groups increased evidently. This increase indicates the variations of the chemical structures of the modified graphene after DNA binding. Only one peak could be fitted at 399.8 eV (-N-C=O), which is from OTA (Fig. 1 (b)). However, the other peak at 400.8 eV is observed (Fig. 1 (d)) after DNA immobilization. It is also present in the strands of P1 along with the peak at 399.8 eV (C-N/N-H groups). In addition, a clear signal of P 2p is observed in the sample after DNA anchoring (Fig. 1 (e)). Therefore, these results prove that P1 has been immobilized on the surface of the amino modified graphene through this feasible method.

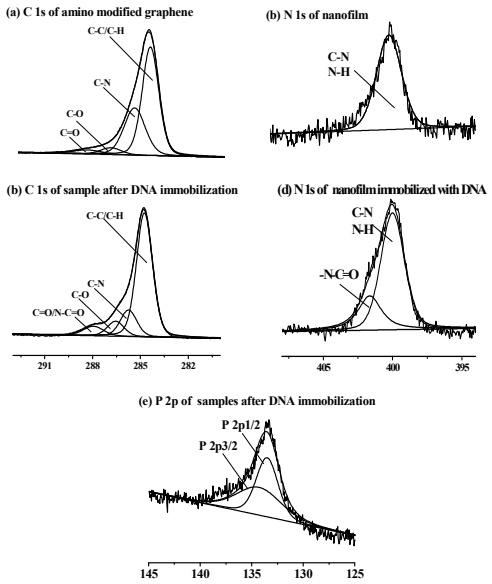

Fig. 1 (a) C 1s, (b) N 1s spectra of nanofilm and (c) C 1s, (d) N 1s, (e) P 2p and (f) S 2p XPS spectra of nanofilm immobilized with DNA.

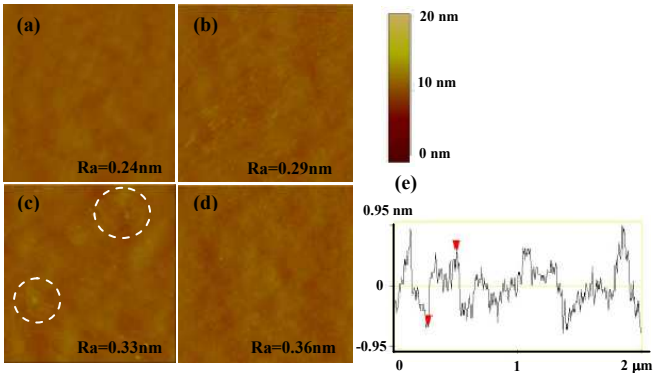

Fig. 2 AFM images of the silicon wafer (a) before and after being self-assembled with (b) OTMS, (c) graphene, and (d) OTA successively.

3.2. Surface morphology of G-NH_2

To investigate the influence of the molecular self-assembly on the surface morphology of the silicon wafers, AFM images were detected and shown in Fig. 2. The surface of the bare silicon wafers is very smooth with an average roughness (*Ra*) of 0.24 nm (Fig. 2 (a)). After the self-assembling of OTMS, *Ra* slightly increased to 0.29 nm with a large amount of particles (Fig. 2 (b)). The graphene sheets appeared on the silicon wafer surface after the self-assembling of graphene, wherein *Ra* is approximately 0.33 nm. The graphene sheets are approximately several hundred nanometers large with irregular shapes with a thickness of approximately 1.18 nm (Fig. 2 (e)). The surface morphology of the nanofilms (Fig. 2 (d)) had a significant change when OTA was self-assembled on the graphene surface. Moreover, the average surface roughness increased to 0.36 nm.

3.3. Electrochemical properties of G-NH_2 before and after DNA immobilization and hybridization

The EIS has been extensively used as an effective and rapid method to measure the impedance value of the electrode surface during the process of the frequency variation [23, 24]. EIS was applied to probe the variations of the amino modified graphene before and after single strand DNA anchoring and double-strand DNA hybridization, in which the solution-based phosphate buffered saline was explored as electrolytes.

The semicircle portion observed at high frequencies corresponds to the electron transfer limiting process (Fig. 3). In the Nyquist diagram, the semicircle diameter of the electrochemical impedance spectroscopy equals to the electron transfer resistance (R_{et}) [25]. The spectra were analyzed using the software Zview2, which uses a nonlinear least-squares fit to determine the parameters of the elements in the equivalent circuit. These spectra were modeled with the Randles equivalent circuit consisting of solution resistance (R_s), charge-transfer resistance (R_{ct}), and constant-phase element (CPE). The simulated R_{et} values of each stage during the self-assembling, DNA anchoring and DNA hybridization are listed in Table 1.

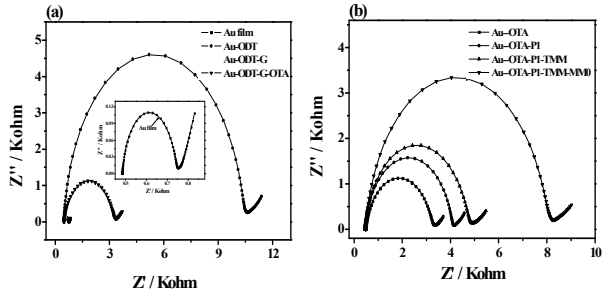

Fig. 3 Nyquist diagrams of (a) the self-assembling processes and (b) DNA immobilization and hybridization onto the surface of G-NH_2. Inset: nyquist diagrams of the Au film.

Table 1 R_{et} values of each stage during the preparation processes of G-NH_2 and DNA immobilization/ hybridization onto the surface.

Each stage	R_{et} (KΩ)
Au film	0.26
Au-ODT	9.79
Au-ODT-G	1.70
Au-ODT-G-OTA	2.58
Au- ODT -G-OTA-P1	3.60
Au- ODT -G-OTA-P1-TMM	4.20
Au- ODT -G-OTA-P1-TMM-MM0	7.40

After ODT was self-assembled onto the surface of gold wafers, the R_{et} value dramatically increased from 0.26 KΩ to 9.79 KΩ (Fig. 3 (a)). This increase suggests that ODT acts as an insulating layer and causes the difficulty in the interfacial electron transfer [26]. While graphene is self-assembled with ODT, the R_{et} value decreases gravely from 9.79 KΩ to 1.70 KΩ. Thus, the presence of graphene could improve the electron transfer because of the restoration of the graphitic network of sp^2 bonds in graphene [27]. After the self-assembling of OTA on the surface of graphene, the R_{et} value increased evidently from 1.70 KΩ to 2.58 KΩ. This increase is attributed to the blocking interaction of OTA on the electron transfer [28].

DNA immobilization and hybridization onto the surface of G-NH_2 was determined by EIS (Fig. 3 (b)). P1 strands could anchor onto the G-NH_2 surface because of the electrostatic interaction between the negative charges of the phosphate groups in DNA strands and the positive charges of the amino groups in G-NH_2. After 100 nM P1 was immobilized, the R_{et} value increased from 2.58 KΩ to 3.60 KΩ. When 100 nM TMM was hybridized with P1, the variation of the R_{et} value is not apparent. This result suggests that TMM did not hybridized with P1 and that no substantially non-specific adsorption between TMM and P1 exists. The R_{et} value continuously increased to 7.40 KΩ after MM0 was hybridized with P1, indicating the formation of double-helix strands between them.

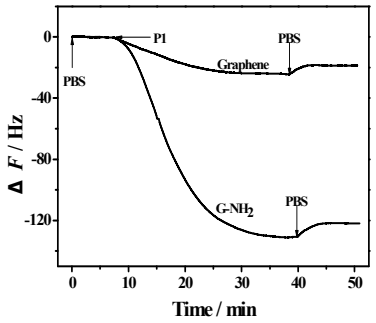

Fig. 4 Frequency shifts changes of the P1-DNA immobilization on G and G-NH_2.

3.4. Adsorbed amount of DNA immobilization and hybridization on G-NH_2

QCM is simple and cost effective. Thus, it has been extensively investigated as a transducer in hybridization based DNA biosensors for the detection of gene mutation [29], genetically modified organisms, [30] and diagnosis of virus [31]. Fig. 4 demonstrates the binding of DNA sequences with the graphene and G-NH_2 films. DNA immobilization reached equilibrium within 30 min after the DNA was circulated into the flow cell for all samples. The systems were allowed to stabilize over 5 min to 10 min periods, and no further significant changes were observed. After the stabilization stage, pure PBS was incubated into the system, which always led to a loss of some unbound DNA from the surface. After a few minutes, the aptamer adhesion level reached a new equilibrium. The ΔF values of the DNA immobilized onto the graphene and G-NH_2 films are 18.63 and 121.57 Hz, respectively. The DNA showed preference to immobilizing onto the G-NH_2 film, which could be due to the high amount of amino groups on the G-NH_2 film.

A typical sensor diagram for the stepwise sensor fabrication and detection is shown in Fig. 5. The variation of the frequency shift of the quartz chip during the procedure of the self-assembling of ODT, graphene, and OTA with the former one successively occurred (Fig. 5 (a)). A first ΔF = -91.5 Hz frequency shift change is found during the circulation of the 10^{-3} M ODT solution after 30 min, i.e., 122.61 ng. This result confirms the successful self-assembling of ODT on the gold surface. The circulation of 0.1 mg/mL graphene suspension into the system caused the decrease in the frequency of QCM chip (161.7 Hz, i.e., 216.68 ng). This result is further explained by the bonding of alkyl chains with graphene within 30 min. After the self-assembling of OTA on the graphene surface, the frequency shift decreased to 66.5 Hz, i.e., 89.11 ng. The continuous decrease of the frequency reveals the self-assembling processes of the small molecules and the intermolecular force.

After the consummation of G-NH_2, label-free P1 was immobilized on the surface. A 121.57 Hz frequency shift change occurred (i.e., 162.90 ng) during the circulation of a 200 nM P1 solution after 40 min (Fig. 5 (b)). This result is attributed to the anchoring of P1 on G-NH_2 because of the electrostatic interaction

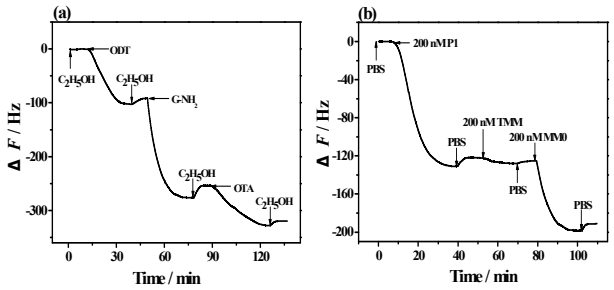

Fig. 5 (a) Frequency shifts changes of the self-assembly processes and (b) Frequency shifts changes of the DNA immobilization and hybridization.

between them. To probe whether or not a non-specific adsorption between the target DNA and the modified graphene exists, the TMM solution was circulated into the system. The circulation of the TMM solution caused only approximately 3.4 Hz drop in frequency within 40 min, thereby proving that a non-specific adsorption occurred between TMM and P1. At last, the circulation of the MM0 solution brought about the frequency decrease of 65.59 Hz, i.e., 87.89 ng, thereby indicating that the MM0 DNA successfully hybridized with P1 on the amino graphene surface.

3.5. Efficiency of P1 immobilization on the G-NH_2 film

The G-NH_2-modified quartz chip was incubated with DNA at various concentrations from 0.1 nM to 200 nM (Fig. 6 (a)) to evaluate the efficiency of the DNA. Using a stepwise increase in the P1 concentration, new equilibrium states associated with a particular oscillation frequency (ΔF) were reached. The oscillation frequency observed after the equilibration of each step allows for a quantitative evaluation of the affinity constant (K_A). If the oscillation frequency is plotted as a function of the DNA concentration, or as the linear version of the Langmuir isotherm, $C_e/\Delta F$ versus C_e, then the affinity constant K_A can be calculated (Fig. 6(b)). The obtained equation is $C_e/\Delta F = (-0.23115) + (-0.01363)\ C_e$ with a regression coefficient of 0.9984. Thus, K_A is 0.059 nM^{-1}, and the saturated adsorbed amount of DNA is 73.37 Hz.

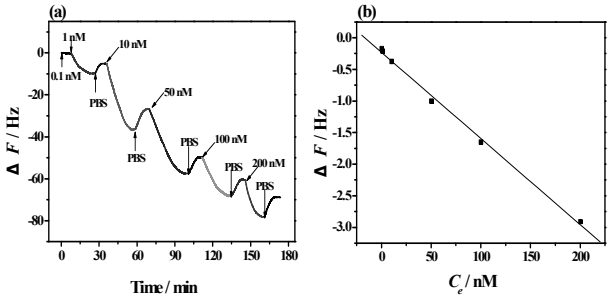

Fig. 6 (a) Frequency response profiles for the immobilization of the P1 at different concentrations of 0.1, 1, 10, 50, 100, and 200 nM. (b) Linear calibration curve for the $C_e/\Delta F$ versus C_e, where C_e is the concentration of the P1.

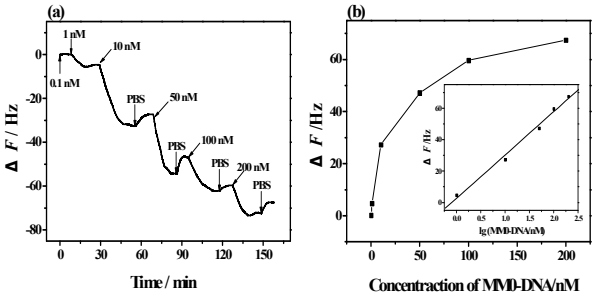

Fig. 7 (a) Frequency response profiles for the hybridization of MM0 at different concentration of 0.1, 1, 10, 50, 100, and 200 nM and (b) Linear calibration curve for ΔF versus Log (C_{MM0}/nM), where C_{MM0} is the concentration of MM0.

3.6. Optimization of target DNA detection

The G-NH_2 modified quartz chip was incubated with MM0 at various concentrations from 0.1 nM to 200 nM (Fig. 7 (a)) to evaluate the efficiency of the DNA biosensor. Using a stepwise increase in the MM0 concentration, new equilibrium states associated with a particular oscillation frequency are reached. The oscillation frequency was observed after the equilibration of each step. If the oscillation frequency is plotted as a function of the MM0 concentration, or as the linear version of the Langmuir isotherm, ΔF versus log (C_e), the limitation of MM0 is obtained (Fig. 7 (b)). The obtained equation is $Y = 2.676 + 27.568 \log X$ (X = concentration of MM0-DNA; $Y = \Delta F$), and the limitation of MM0 is 0.8 nM. The other test motheds were summarized in table 2, compared with other detection limit, this value is good, thereby indicating that G-NH_2 is suitable for DNA biosensor.

Table 2 Different test methods and the detection limit.

Detection Technology	Linear range	LOD	References
Quartz crystal balance	86 - 468 ng/ml	86 ng/ml	34
EIS measurement	0.2 μM-50 nM	20 nM	35
differential pulse voltammetry	0 - 225 pM	1 pM	36
surface plasmon resonance	0.12 - 120 nM	10 nM	37
Differential pulse voltammograms	0.5 -10 nM	0.085 nM	38
Fuorescence	1.4 – 92 nM	2 nM	39

Conclusions

The self-assembling technology and intermolecular interaction approach were applied to fabricate the G-NH_2 sensitive layer for DNA biosensor. The variation of C 1s and N 1s XPS signals during the procedure of the self-assembling could prove the close bonding of the small molecules and graphene onto the substrates. Moreover, the observation of P 2p signal of the modified G-NH_2 after DNA immobilization indicates the feasibility of G-NH_2 application as the sensitive layer for the

DNA biosensor. The similar change of the electrochemical properties and surface morphology of G-NH_2 layer at the different stages were also be obtained by EIS and AFM. Herein, the bonding amounts of ODT, graphene, and OTA on Au substrates are 122.61, 216.68 and 89.11 ng, respectively, which was determined by QCM in situ. The detection limitation of MM0 is approximately 0.8 nM, which was deduced through the approach of the concentration titration. Therefore, G-NH_2 prepared through this simple and feasible way could be used as the sensitive layer for DNA biosensor.

Acknowledgments

This work was supported by Program for the National Natural Science Foundation of China (NSFC: Account No. 51173172 and 21104070).

Author information

Corresponding author
*E-mail addresses: mainzhh@163.com
[1]Henan Provincial Key Laboratory of Surface and Interface Science,
[2]Henan Collaborative Innovation Center of Environmental Pollution Control and Ecological Resoration,
Zhengzhou University of Light Industry, No. 166, Science Avenue, Zhengzhou 450001, P. R. China.

References

1 M. D. Stoller, S. Park, Y. Zhu, J. An and R. S. Ruoff, *Nano Lett.*,2008, **8**, 3498-3502.
2 W. Hu, C. Peng, M. Lv, X. Li, Y. Zhang, N. Chen, C. Fan and Q. Huang, *ACS Nano,* 2011, **5**, 3693-3700.
3 J. Liang, Z. Chen, L. Guo and L. Li, *Chem. Commun.,* 2011, **47**, 5476-5478.
4 M. Kalbacova, A. Broz, J. Kong and M. Kalbac, *Carbon,* 2010, 48, 4323-4638.
5 H. Yang, F. Li, C. Shan, D. Han, Q. Zhang, L. Niu and A. Ivaska, *J. Mater. Chem.* 2009, **19**, 4632-4638.
6 H. Bai, Y. Xu, L. Zhao, C. Lia and G. Shi, *Chem. Commun.,* 2009, 1667-1669.
7 C. Shan, H. Yang, D. Han, Q. Zhang, A. Ivaska and L. Niu, *Langmuir,* **2009**, *25*, 12030-12033.
8 K. J. Huang, D. J. Niu, X. Liu, Z. W. Wu, Y. Fan, Y. F. Chang and Y. Y. Wu, *Electrochim. Acta,* 2011, 56, 2947-2953.
9 F. OuYang, B. Huang, Z. Li, J. Xiao, H. Wang and H. Xu, *J. Phys. Chem. C,* 2008, **112**, 12003-12007.
10 L. S. Zhang, X. Q. Liang, W. G. Song and Z. Y. Wu, *Phys. Chem. Chem. Phys.,* 2010, **12**, 12055-12059.
11 X. Zhang, J. Yin, C. Peng, W. Hu, Z. Zhu, W. Li, C. Fan and Q. Huang, *Carbon,* 2011, **49**, 986-995.
12 H. Yin, Y. Zhou, Q. Ma, S. Ai, Q. Chen and L. Zhu, *Talanta,* 2010, **82**, 1193-1199.
13 J. Li, J. Chen, X. Zhang, C. Lu and H. Yang, *Talanta,* 2010, **83**, 553-558.
14 J. Lu, I. Do, L. T. Drzal, R. M. Worden and I. Lee, *ACS Nano,* 2008, **2**, 1825-1832.
15 C. Sanchez, B. Julian, P. Belleville and M. Popall, *J. Mat. Chem.,* 2005, **15**, 3559-3592.
16 O. Parlak, A. Tiwari, A. P. F. Turner and A. Tiwari, *Biosens. Bioelectron.,* 2013, **49**, 53-62.
17 Y. Fang, S. Guo, C. Zhu, Y. Zhai and E. Wang, *Langmuir,* 2010, **26**, 11277-11282.
18 J. Shen, Y. Hu, C. Li, C. Qin, M. Shi and M. Ye, *Langmuir,* 2009, **25**, 6122-6128.
19 H. Yang, C. Shan, F. Li, D. Han, Q. Zhang and L. Niu, *Chem. Comm.*, 2009, 3880-3882.
20 K. Huang, D. Niu, X. Liu, Z. Wu, Y. Fan, Y. Chang, Y. Wu, *Electrochim. Acta,* 2011, **56**, 2947-2953.
21 Q. Chen, H. J. Yan, C. J. Yan, G. B. Pan, L. J. Wan, G. Y. Wen and D. Q. Zhang, *Surf. Sci.,* 2008, **602**, 1256-1266.
22 H. Gu, Y. Yu, X. Liu, B. Ni, T. Zhou and G. Shi, *Biosens. Bioelectron.,* 2012, **32**, 118-126.
23 S. Suzuki, A. Nakajima, M. Sakai, J. H. Song, Yoshida, Y. Kameshima, and K. Okada, *Surf. Sci.,* 2006, **600**, 2214-2219.
24 T. Zhang, Z. Cheng, Y. Wang, Z. Li, Y. Li, and Y. Fang, *Nano Lett.,* 2010, **10,** 4738-4741.
25 B. Piro, J. Haccoun, M. C. Pham, L. D. Tran, A. Rubin, H. Perrot, and C. Gabrielli, *J. Electroanal. Chem.,* 2005, **577,** 155-165.
26 C. Tlili, H. Korri-Youssoufi, L. Ponsonnet, C. Martelet, and N. J. Renault, *Talanta,* 2005, **68**, 131-137.
27 C. Jiang, T. Yang, K. Jiao, and H. Gao, *Electrochim. Acta*, 2008, **53**, 2917-2924.
28 D. Yu, J. Tian, J. Dai, and X. Wang, *Electrochim. Acta,* 2013, **97**, 409-419.
29 C. Mattevi, G. Eda, S. Agnoli, S. Miller, K. A. Mkhoyan, O. Celik, D. Mastrogiovanni, G. Granozzi, E. Garfunkel, and M. Chhowalla, *Adv. Funct. Mater.,* 2009, **19**, 2577-2583.
30 V. Chukharev, T. Vuorinen, A. Efimov, and N. V. Tkachenko, *Langmuir,* 2005, **21**, 6385-6391.
31 X. Su, R. Robelek, Y. Wu, G. Wang, and W. Knoll, *Anal. Chem.,* 2004, **76**, 489-494.
32 I. Mannelli, M. Minunni, S. Tombelli, and M. Mascini, *Bioelectron.,* 2003, **18**, 129-140.
33 C. Yao, T. Zhu, J. Tang, R. Wu, Q. Chen, M. Chen, B. Zhang, J. Huang, and W. Fu, *Biosens. Bioelectron.,* 2008, **23**, 879-885.
34 K.S. Chen, S. C. Chen, H. R. Lin, T. R. Yan, and C. C. Tseng, *Mat. Sci. Eng. C*, 2007, **27**, 716–724.
35 H. Gu, X. Su, and K. Loh, *J. Phys. Chem. B* 2005, 109, 13611-13618.
36 N. Zhu, Z. Chang, P. He, and Y. Fang, *Electrochim. Acta,* 2006, **51**, 3758–3762.
37 T. Livache, E. Maillart, N. Lassalle, P. Mailley, B. Corso, P. Guedon, A. Roget, abd Y. Levy, *J. Pharmaceut. Biomed.*, 2003, **32**, 687-696.
38 H. Qi, X. Li, P. Chen, and C. Zhang. *Talanta*, 2007, **72**,1030-1035.
39 Z. Wu, J. Jiang, L. Fu, G. Shen, and R. Yu, Anal. Biochem., 2006, **353**, 22–29.

Cite this: DOI: 10.1039/c0xx00000x

www.rsc.org/xxxxxx

ARTICLE TYPE

JPEG format:

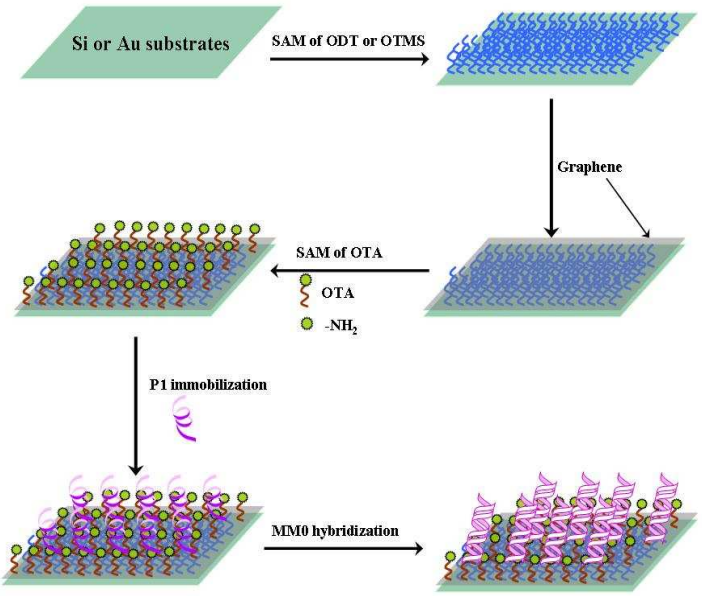

Scheme 1 Schematic diagram of DNA immobilization/ hybridization onto the surface of G-NH_2 via the intermolecular force.

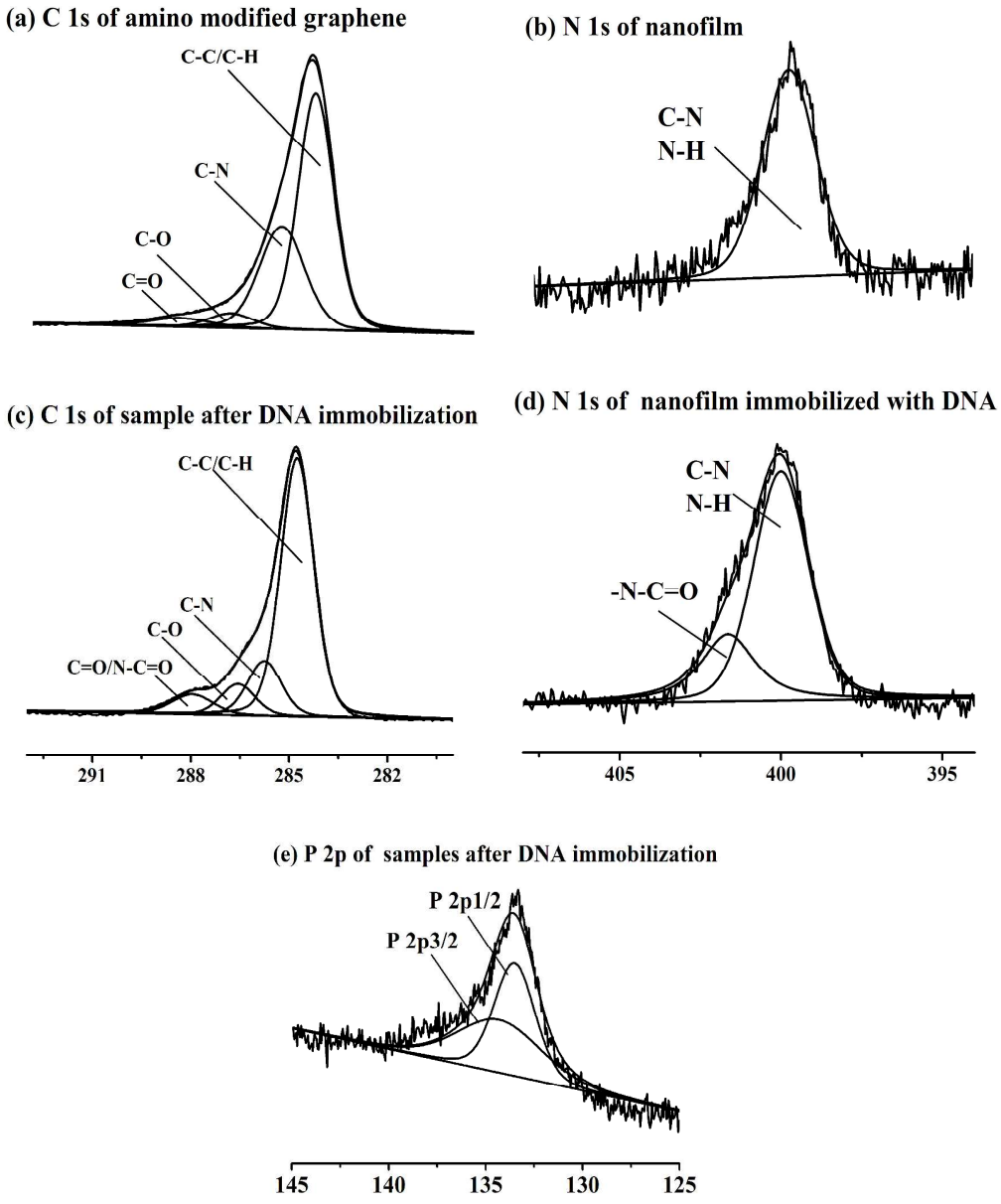

Fig. 1 (a) C 1s, (b) N 1s spectra of nanofilm and (c) C 1s, (d) N 1s, (e) P 2p and (f) S 2p XPS spectra of nanofilm immobilized with DNA.

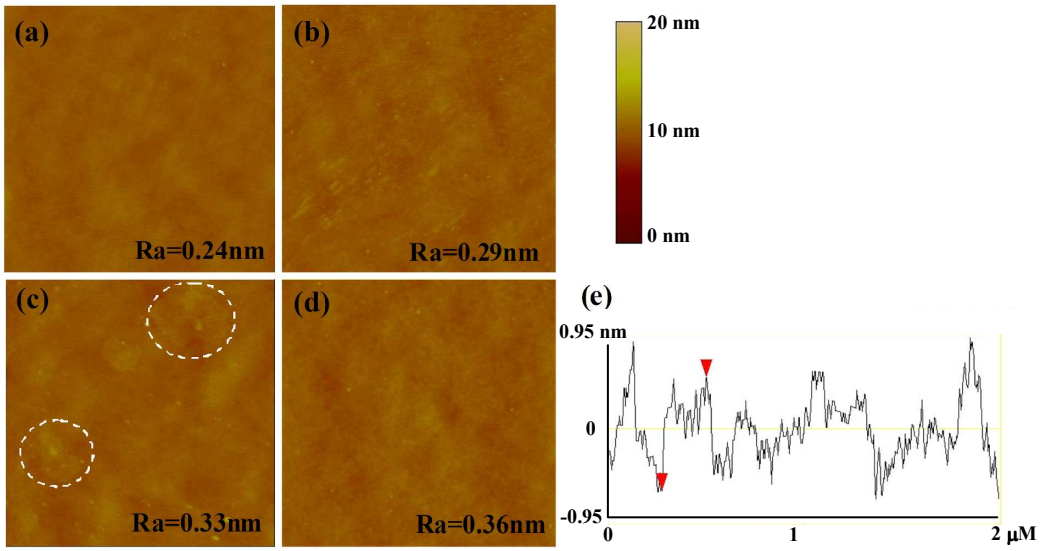

Fig. 2 Two-dimensional AFM images of the silicon wafer (a) before and after being self-assembled with (b) OTMS, (c) graphene, and (d) OTA successively.

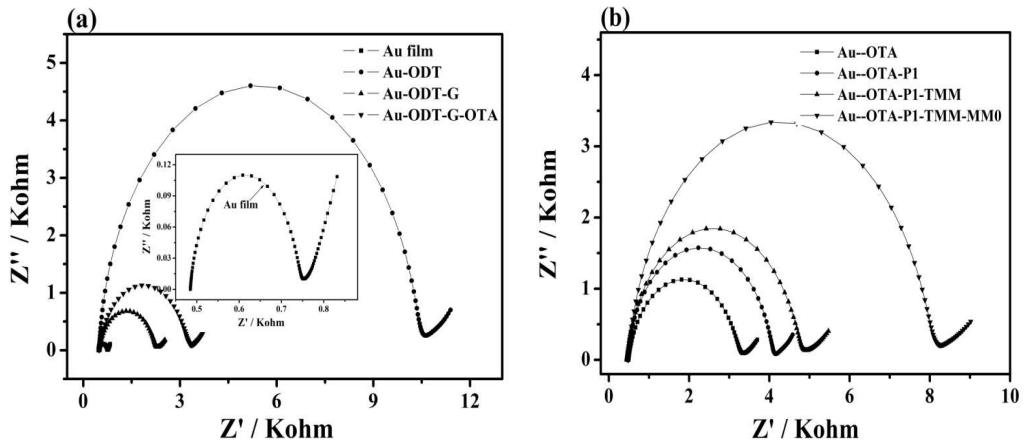

Fig. 3 Nyquist diagrams of (a) the self-assembling processes and (b) DNA immobilization and hybridization onto the surface of G-NH_2. Inset: nyquist diagrams of the Au film.

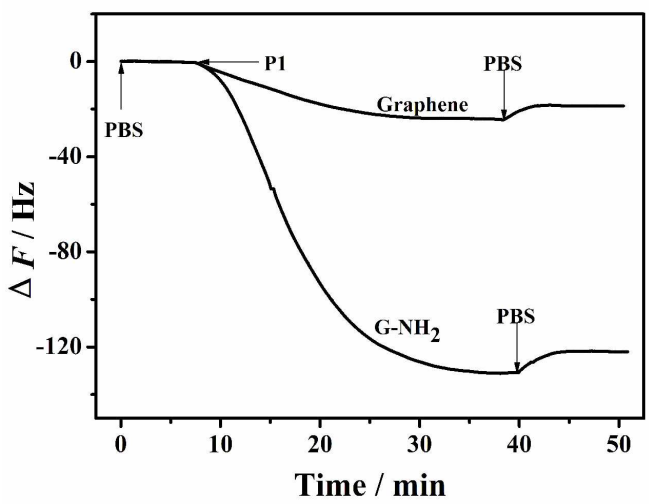

Fig. 4 Frequency shifts changes of the P1-DNA immobilization on G and G-NH_2.

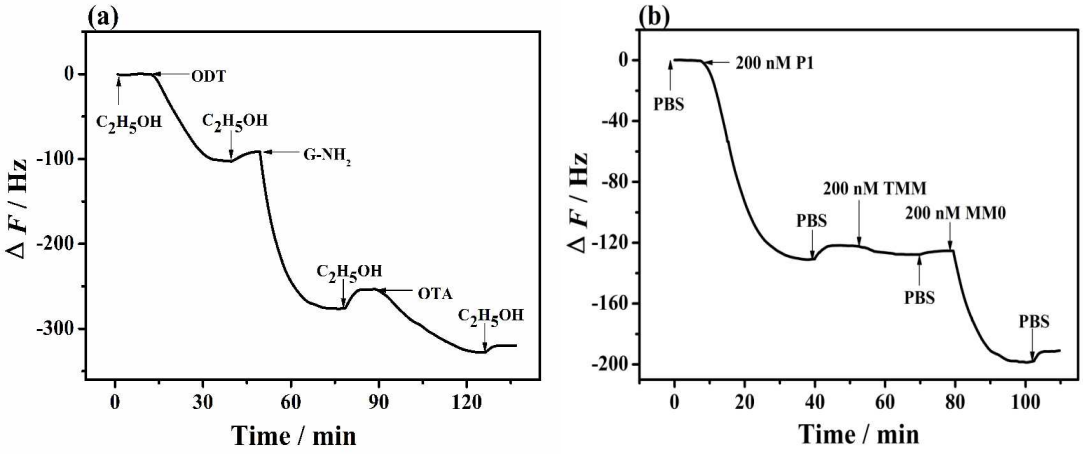

Fig. 5 (a) Frequency shifts changes of the self-assembly processes and (b) Frequency shifts changes of the DNA immobilization and hybridization.

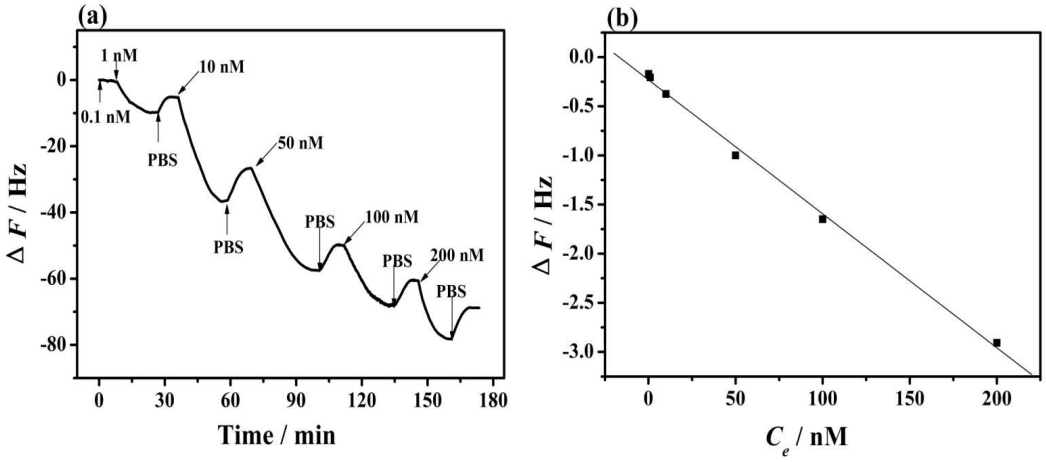

Fig. 6 (a) Frequency response profiles for the immobilization of the P1 at different concentrations of 0.1, 1, 10, 50, 100, and 200 nM. (b) Linear calibration curve for the $C_e/\Delta F$ versus C_e, where C_e is the concentration of the P1.

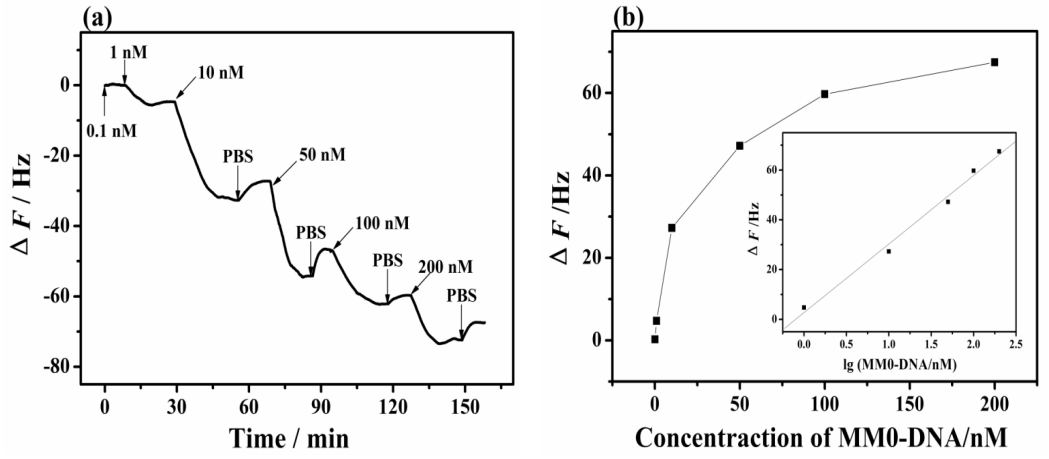

Fig. 7 (a) Frequency response profiles for the hybridization of MM0 at different concentration of 0.1, 1, 10, 50, 100, and 200 nM and (b) Linear calibration curve for ΔF versus Log (C_{MM0}/nM), where C_{MM0} is the concentration of MM0.

A table of contents entry：

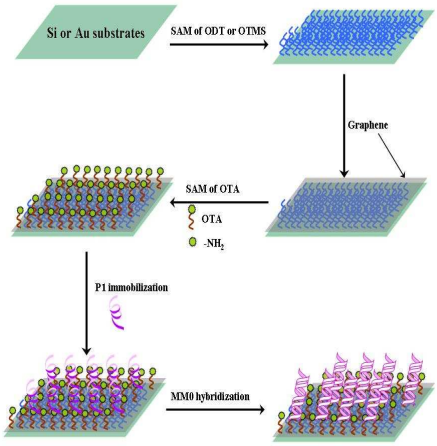

The self-assembly method was used to prepare amino functionalized graphene and it was used in DNA biosensors.